Wojciechowski, Jarosław; Kolanowski, Łukasz; Graś, Małgorzata; Szubert, Karol; Bund, Andreas; Fic, Krzysztof; Lota, Grzegorz:

Anti-corrosive siloxane coatings for improved long-term performance of supercapacitors with an aqueous electrolyte

Original published in: Electrochimica acta / International Society of Electrochemistry New York, NY [u.a.] : Elsevier. - 372 (2021), art. 137840, 15 pp.

Original published: 2021-01-29

ISSN: 0013-4686

DOI: 10.1016/j.electacta.2021.137840

[*Visited:* 2021-09-17]

Electrochimica Acta 372 (2021) 137840

Contents lists available at ScienceDirect

Electrochimica Acta

journal homepage: www.elsevier.com/locate/electacta

Anti–corrosive siloxane coatings for improved long–term performance of supercapacitors with an aqueous electrolyte

Jarosław Wojciechowski[a], Łukasz Kolanowski[a], Małgorzata Graś[a], Karol Szubert[b], Andreas Bund[c], Krzysztof Fic[a,*], Grzegorz Lota[a,*]

[a] Poznan University of Technology, Institute of Chemistry and Technical Electrochemistry, Berdychowo 4, Poznan 60–965, Poland
[b] Adam Mickiewicz University, Faculty of Chemistry, Umultowska 89b, Poznan 61–614, Poland
[c] Technische Universität Ilmenau, Electrochemistry and Electroplating Group, Gustav–Kirchhoff–Straße 6, Ilmenau 98693, Germany

ARTICLE INFO

Article history:
Received 27 July 2019
Revised 15 September 2020
Accepted 19 January 2021
Available online 29 January 2021

Keywords:
Corrosion
Electrochemical capacitors
Siloxane coatings
Stainless steel

ABSTRACT

This paper reports on the impact that the corrosion of the stainless steel current collectors has on the performance fade of a symmetric, carbon/carbon electrochemical capacitor, operating with an aqueous electrolyte (1 M Na_2SO_4). The results obtained by applying electrochemical ageing protocols (voltage–holding tests) confirm that the current collector of the positive electrode undergoes tremendous degradation during 200 h in the charged state. To prevent the detrimental impact of the corrosion, a hydrophobic siloxane coating has been successfully applied. In the case of siloxane–protected current collectors that are subjected to identical ageing protocols, no significant deterioration in the electrochemical capacitor performance was observed. The siloxane coating reduces the electrochemical corrosion rate of 316 L stainless steel significantly, as the potentiodynamic polarization tests and the electrochemical impedance spectroscopy results show. The presence of the coating is demonstrated by the water contact angle measurements, atomic force microscopy and energy–dispersive X–ray spectroscopy analysis.

1. Introduction

Electrochemical capacitors (often called supercapacitors or ultracapacitors) are devices capable of storing electric energy in the electrical double–layer, which is formed at the electrode/electrolyte interface. In certain cases, the electrostatic charge accumulation mechanism might be enhanced by faradaic reactions, resulting in the so–called pseudocapacitive effect [1-9]. Since the electrode material that is most often applied is activated carbon with a well–developed specific surface area (up to 2500 $m^2 \cdot g^{-1}$), the number of the charges stored is much higher than in the case of conventional electric or electrolytic capacitors, such as film, polymer or aluminium electrolytic capacitors (capacitance in the order of micro- and millifarads), offered by, e.g., Panasonic Industry Europe GmbH [10-12]. As the capacitance of the electrical double–layer ranges from 10–50 $\mu F \cdot cm^{-2}$, the specific capacitance of carbon–based devices reaches several hundred farads per gram of active electrode material. The lack or negligible contribution from the faradaic reactions to the charge storage mechanism means that these devices can be charged and discharged even in milliseconds [13]. Therefore, supercapacitors are characterized by extremely high specific power. However, the electrostatic origin of the charge storage results in a relatively low specific energy and remarkable self–discharge [3,4,14-20]. Nonetheless, no charge transfer and structural change in the electrode material (at least in principle) has a significant impact on the lifetime of these devices; unlike batteries, they can operate for up to 500 000 cycles, even when they are fully discharged each time [3].

The most commonly applied electrode materials, besides activated carbon, are aerogels, carbon nanotubes and sometimes graphene–related structures [3,4,6,7,14,21-23]. The use of aqueous and organic electrolytes limits the operating voltage to ca. 1 V and 2.5 V, respectively. In the first case, the voltage is limited by the electrochemical stability of water. Aqueous solutions of inorganic salts (e.g., Na_2SO_4) are capable of delivering an operating voltage of 1.6 V, or even more (up to 2.0 V) if the cell is optimized [6,23-27]. The prominent role of the electrolyte in electrochemical capacitor applications has been widely discussed elsewhere [28-33].

Capacitive technologies usually demonstrate an excellent long–term performance and in–depth research on novel materials with

* Corresponding authors.
E-mail addresses: krzysztof.fic@put.poznan.pl (K. Fic), grzegorz.lota@put.poznan.pl (G. Lota).

https://doi.org/10.1016/j.electacta.2021.137840

great stability over thousands of cycles is still performed. Nevertheless, activated carbons (and carbon–based materials) seem to be the most suitable candidates. However, the mechanisms governing their ageing and performance fade are still under intensive investigation [23,25,34-39]. It seems that the degradation of the electrode porosity, preceded by carbon oxidation and electrolyte decomposition, remains at the origin of the fading performance [23,24,39]. One should, however, keep in mind that electrode degradation might only be part of the ageing factors.

Recently, the interest in the ageing aspects has been re–orientated from the (electro)chemical stability of the electrode materials to the other cell components. These efforts are focused on the corrosion process of current collectors or case elements (which are in direct contact with the electrolyte solution and the active electrode material) and its corresponding impact on the working parameters of energy storage devices [6,40-42]. At open circuit conditions, i.e., at steady–state (or equilibrium) conditions, oxidation and reduction reactions occur on the surface of the metal (or stainless steel) immersed in the aqueous electrolyte. Metal is oxidized to form ions, while species such as O_2 or H_3O^+ are being reduced [43-47]. Both reactions proceed at an equal rate, until the system is not externally polarized. During the charging step, the redox processes start to proceed faster. At open circuit conditions, as well as during polarization, the ions from the current collector surface start to pass into the electrolyte solution. Przygocki et al. [48] found that these ions are actively involved in charging the electrical double–layer at the electrode/electrolyte interface. Additionally, it seems that a passive oxide film is formed on the surface of stainless steel current collectors. In the case of 316 L stainless steel, its composition varies depending on the pH of the electrolyte solution. Over time, the current collector undergoes progressive degradation, and this process significantly affects the performance of the electrochemical capacitor [6].

The techniques used to protect metals from corrosion focus primarily on the use of corrosion inhibitors, cathodic protection and various types of coatings, e.g., metallic and organic [43-47]. The use of chromate–based coatings (so–called conversion coatings) was one of the most frequently used and effective anti-corrosive protection measures [46]. However, the carcinogenic properties of hexavalent chromium reduced their applications [49-51]. In recent years, increasing attention has been paid to organosilicon coatings, which are organic–inorganic hybrids. Their structure contains a silicon atom that can form bonds with both organic moieties and inorganic substrates [49-71]. The siloxane coating is deposited by immersing the metal in an aqueous or non–aqueous sol–gel solution containing organosilicon compounds. In such a solution, hydrolysis and condensation reactions occur [50,51]. The alkoxy groups ($\equiv$Si–O–$(CH_2)_n$–CH_3) with water molecules and hydroxyl moieties, which are prevalent on the surface of the metal (metal–OH), create $\equiv$Si–OH and metal–O–Si$\equiv$ bonds, respectively. Then, as a result of the condensation reaction between the $\equiv$Si–OH and metal–OH groups, metal–O–Si$\equiv$ bonds and a well–developed, cross–linked network made of –O–[Si–O]$_n$–Si$\equiv$ bonds are formed. The resulting coating is attached to the substrate (metal–O–Si$\equiv$). The presence of a hydrophobic alkyl chain makes the surface more resistant to aggressive aqueous electrolytes [50,51]. Furthermore, the presence of various functional groups in the structure of the organosilicon compound makes the siloxane coating a good base for applying subsequent layers of various types of other coatings.

This paper reports on the influence of a siloxane coating on the corrosion behaviour of 316 L stainless steel current collectors and, thus, on the working parameters of symmetric carbon/carbon electrochemical capacitors. The electrochemical performance has been verified by different types of electrochemical techniques (cyclic voltammetry, galvanostatic cycling, electrochemical impedance spectroscopy). Additionally, the surface morphology and properties for bare, unmodified and modified with deposited siloxane coating 316 L stainless steel current collectors were estimated using Atomic Force Microscopy (AFM), energy–dispersive X–ray spectroscopy and water contact angle (WCA) measurements. All the electrochemical tests were performed in aqueous 1 M Na_2SO_4, which is one of the most frequently applied aqueous electrolytes in the research on electrochemical capacitors due to its specific properties [6]. When comparing aqueous and organic electrolytes, it is certain that the former are characterized by a lower price, greater safety in terms of work and service for human life and health and, equally important, for the environment. Moreover, the influence of the organic electrolyte on the corrosion of the current collectors in electrochemical capacitors and lithium–ion batteries is also undeniable [72-75]. In our opinion, based on the above discussion, the aim of the research we have undertaken is valid.

2. Experimental

2.1. Surface treatment

316 L stainless steel (nominal composition: $\leq$0.03 wt–% C, $\leq$1.0 wt–% Si, $\leq$2.0 wt–% Mn, max 0.045 wt–% P, $\leq$0.015 wt–% S, $\leq$0.11 wt–% N, 16.5–18.5 wt–% Cr, 2.0–2.5 wt–% Mo, 10.0–13.0 wt–% Ni) rods (diameter of 12 mm) and discs (diameter of 28 mm) were used as the current collectors, on which siloxane coatings were deposited. First, these rods, as well as the 316 L stainless steel discs were degreased in acetone, dried in air and then placed in a hot (85 °C) 10% KOH solution for 15 min to remove contaminants and to activate the surface, i.e., to form as many hydroxyl groups as possible. After rinsing and drying in an oven (80 °C, 30 min), the samples were placed in an aqueous solution (pH 4), containing 20 mL of octyltriethoxysilane (OTES), 11 mL of tetraethoxysilane (TEOS), 33 mL of methanol and acetic acid for 15 min. To obtain a well dispersed sol–gel, the solution was stirred for 72 h at 25 °C and then placed in an ultrasonic bath. After that, the samples with the siloxane coating were dried vertically in an oven at 80 °C for 1 h. Bare current collectors, which were pre–treated in a hot (85 °C) 10% KOH solution, were aged in air to create a stable, thin passive oxide film.

In the next step, the electrode material, which contained 85% activated carbon (Norit® GSX, Alfa Aesar), 10% binder polytetrafluoroethylene (Sigma–Aldrich) and 5% acetylene carbon black (Super C65, Imerys), was prepared in the form of pellets (12 mm in diameter). The obtained carbon composite electrodes (11.5 mg) were used to prepare symmetric electrochemical capacitors (ECs) in Swagelok® cell systems together with bare and with modified 316 L stainless steel current collectors (Fig. 1). The carbon composite electrodes, as well as the separators were soaked in 250 µL of a 1 M Na_2SO_4 electrolyte solution.

2.2. Analysis of the surface

An atomic force microscope (AFM, Keysight 5500), FEI Quanta 250 FEG microscope equipped with an energy–dispersive X–ray spectroscopy (EDS) detector and an instrument for measuring the surface water contact angle (WCA) Krüss GmbH (model DSA 100 Expert), equipped with a fully automated dosing system were used for the physicochemical analysis of the surface of the 316 L stainless steel and deposited siloxane coating.

AFM images of the bare and coated 316 L stainless steel samples were taken, and the thickness of the obtained anti–corrosive coating was determined. The surface of the coating was scratched with the sharp edge of an aluminium sheet. As stainless steel is harder

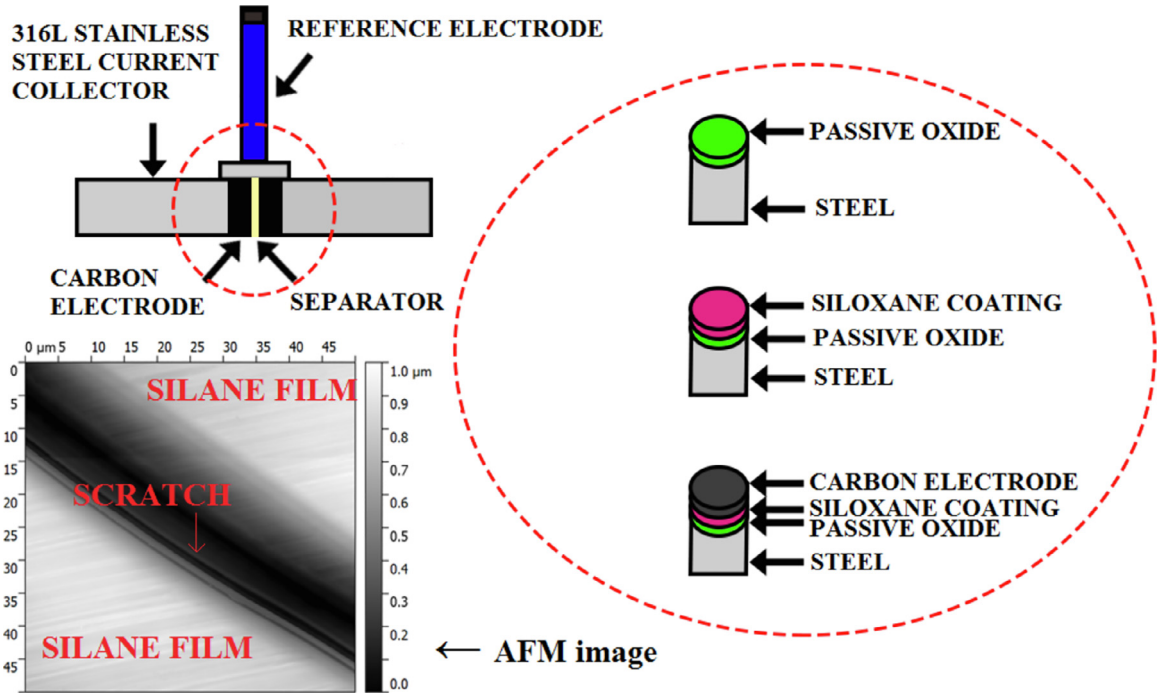

Fig. 1. Schematic representation of the Swagelok® three–electrode cell system for testing electrochemical capacitors with an image of a 316 L stainless steel surface covered with a siloxane coating. (For interpretation of the references to colour in this figure legend, the reader is referred to the web version of this article.)

than aluminium, it can be assumed that only the siloxane layer has been scratched. To obtain more reliable results, two cross–section profiles through the resulting scratch were made. The thickness of the tested coating was determined on the basis of the height histogram.

The water contact angle (WCA) of the surface of the 316 L stainless steel and the steel with the deposited siloxane coating was determined. The average value of three randomly selected surface locations were taken into account. Measurements were made on the basis of water drop shape analysis.

2.3. Electrochemical measurements

316 L stainless steel discs (28 mm in diameter) with and without a siloxane coating were subjected to electrochemical measurements in a three–electrode Plexiglas® cell system (corrosion testing). The modified and unmodified steel discs were used as working electrodes, while a mercury–mercury sulphate electrode (MSE) ($Hg|Hg_2SO_4||K_2SO_4$ (0.5 M)) and a platinum disc served as the reference and counter electrodes, respectively. All electrochemical tests were performed in a 1 M Na_2SO_4 solution. First, the open circuit potential (OCP) was measured for 240 min. Then, a potentiodynamic polarization (PP) test was performed. The working electrode was polarised first cathodically and then anodically to ±0.250 V with respect to the initial OCP value. The scan rate was 0.2 $mV \cdot s^{-1}$. Potentiostatic electrochemical impedance spectroscopy (PEIS) was performed on fresh samples, which were immersed in a 1 M Na_2SO_4 solution for 240 min. The amplitude and the frequency range of the applied signal were equal to ±10 mV vs. OCP and 100 kHz – 10 mHz, respectively.

To assess the influence of the siloxane coating on the performance of electrochemical capacitors (EC), two– and three–electrode Swagelok® cell systems (Fig. 1) were subjected to electrochemical measurements, i.e., cyclic voltammetry (CV), galvanostatic charging/discharging (GCD), potentiostatic electrochemical impedance spectroscopy (PEIS) and long–term ageing measurements. In the case of PEIS, the applied signal amplitude and frequency range were equal to ±5 mV vs. OCP and 100 kHz – 10 mHz, respectively. On the basis of the leakage current (minimal value of the current density that is needed to maintain the applied cell voltage) technique, a value of 1.8 V was established as the applied voltage for every two–electrode Swagelok® cell test. The long–term ageing measurements procedure consists of three different electrochemical techniques, as reported in [15]. However, for the present study, the procedure has been upgraded and became more rigorous. Therefore, the two–electrode cells were charged to 1.8 V using the direct current technique with a constant current density (GC) value (1 $A \cdot g^{-1}$). This voltage value was maintained for 5 h (floating). After that, three cycles of galvanostatic charge/discharge measurements were performed, and then the circuit was opened for 30 min. Finally, potentiostatic electrochemical impedance spectroscopy (PEIS) was performed. This cycle (→GC→floating (5 h)→GCD (3 cycles)→OCP→PEIS) was repeated 10 times. Therefore, the electrochemical capacitors were fully charged for 50 h.

In fact, three long–term ageing procedures were applied (in three series). The second one was the same. The third one was twice as long. Thus, the loop was repeated 20 times, i.e., the electrochemical capacitors were fully charged for 100 h. Globally, during the three procedures, the electrochemical capacitors were constantly fully charged (1.8 V) for 200 h ($50h + 50h + 100h$). After the first and second procedure, two–electrode Swagelok® cell systems were maintained at OCP for 24 h. After the third one, for one week. After this time, three– and two–electrode CV, PEIS and GCD tests were performed. All tests were carried out at ambient conditions, using an electrochemical workstation potentiostat/galvanostat VMP3 (biologic, France) with an impedance module. Table 1 presents the nomenclatures of all the tested species. It is worth mentioning again that two types (rods and discs) of 316 L stainless steel species were analysed. The rods were used as current collectors in electrochemical capacitor testing, while the discs were used for the corrosion testing.

Table 1
Nomenclature of all samples subjected to corrosion, as well as electrochemical capacitor studies.

316 L stainless steel surface modification	Diameter (mm)	Testing	Signature
Bare disc	28	Corrosion	316 L/28
Siloxane coating	28	Corrosion	SC/28
Bare current collector	12	EC	316 L/12
Siloxane coating	12	EC	SC/12

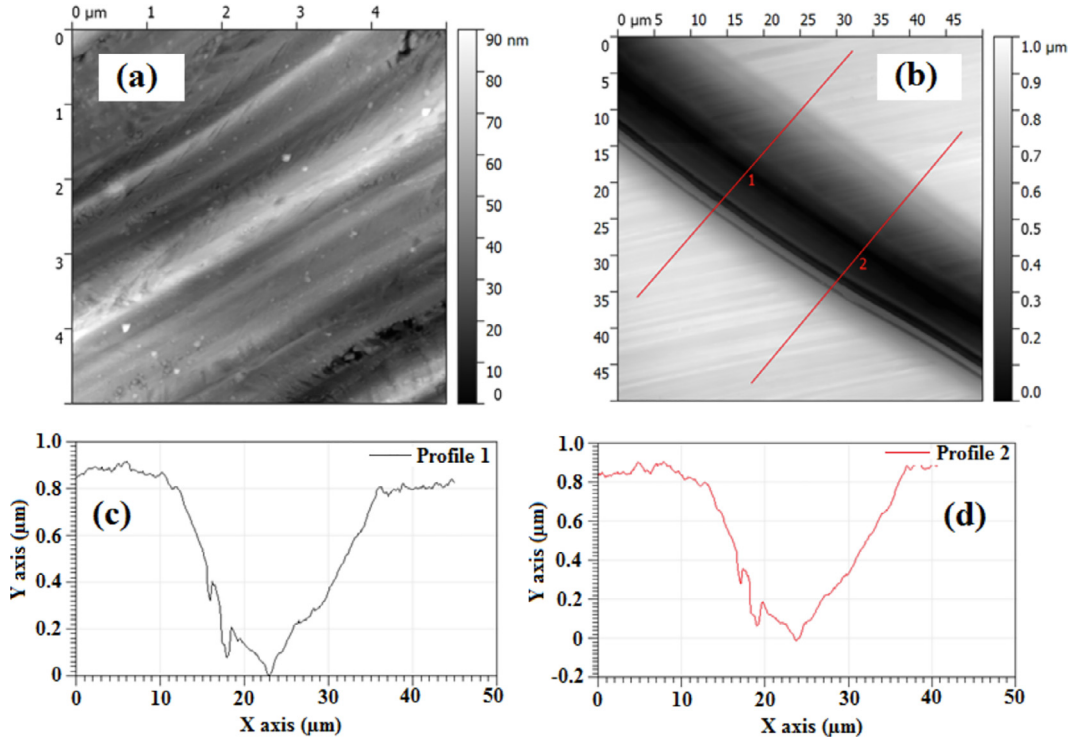

Fig. 2. (a) AFM image of bare 316 L stainless steel, (b) AFM image of a deposited siloxane coating with a scratch and two cross section profiles marked, and (c–d) height histograms of two profiles through the scratch.

3. Results and discussion

3.1. Analysis of the surface

Fig. 2(a–d) shows atomic force microscope (AFM) images of the 316 L stainless steel surface with and without the deposited siloxane coating, the cross–sectional profiles through the scratches made on the surface of coating and the height histograms of the mentioned profiles. The thickness of the coating is ca. 800 nm.

The value of the WCA of the bare 316 L stainless steel of 81° indicates a quite hydrophilic surface. The situation is quite different for the sample with the siloxane coating; the surface is more hydrophobic, as the contact angle value is 95° In the aqueous sol–gels, Si–OH bonds are formed as a result of the hydrolysis reaction of the alkoxy groups (Si–O–CH_2CH_3). Due to the condensation reaction between the two Si–OH moieties, a well–developed, cross–linked siloxane network containing –O–[*Si*–O]$_n$–Si– moieties is created [50-52].

The reactions between hydroxyl groups prevalent on the surface of the steel (metal–OH) and the Si–OH or Si–O–CH_2CH_3 moieties form metal–O–Si covalent bonds, and the siloxane coating is firmly attached to the steel surface. The presence of an alkyl chain at the silicon atoms makes the surface more hydrophobic, i.e., resistant to aggressive aqueous electrolytes. Certainly, the pH of the sol–gel has a significant effect on the rate of the two above reactions. If the pH is acidic or alkaline, the hydrolysis and condensation reactions occur faster and more Si–OH and –O–[*Si*–O]$_n$–Si bonds are formed [50-52]. Therefore, the coating is thicker and more porous. In the case of a non–aqueous solution, the only source of water molecules is the organic solvent (e.g., methanol). As a result, much fewer Si–OH bonds are formed and, thus, less –O–[*Si*–O]$_n$–Si– [50-52]. However, as is well–known, in acidic solutions, the dissolution reactions of metals, steels and alloys are much faster than in neutral solutions. It has already been stated that only in solutions with neutral pH values is there a formation of the thermodynamically most stable passive oxide film on the surface of the 316 L stainless steel [6]. Most likely, during the deposition process from an acidic solution, the 316 L stainless steel surface could be attacked. Our previous works [50,51] clearly indicate that coatings deposited from non–aqueous solutions are characterized by higher water contact angle values and more anodic corrosion potential, while coatings derived from acidic solutions are definitely thicker; thus, they slow down the corrosion process to a greater extent (lower corrosion current density value). The coating deposited from the non–aqueous solution, although thinner, is more compact, and more metal–O–Si bonds are formed. However, with regard to the purpose of the obtained coating, it is not the intention to use an extremely hydrophobic coating. A thicker and more porous one that is capable of adsorbing the electrolyte solution is more desirable when it is used to protect the steel current collectors in an electrochemical capacitor.

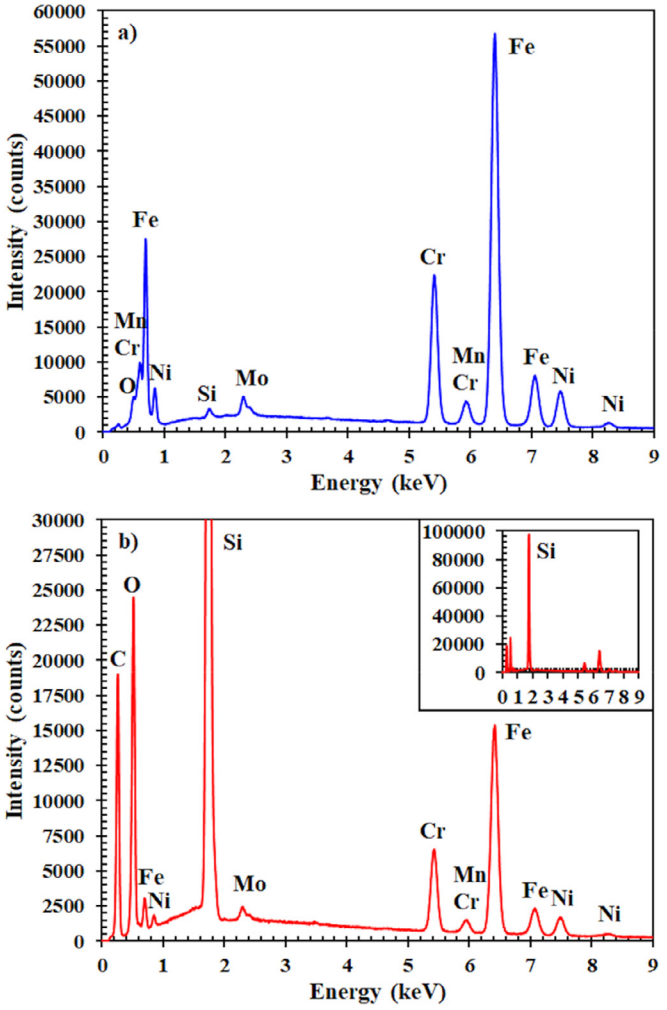

Fig. 3. Energy–dispersive X–ray spectroscopy (EDS) results of (a) bare 316 L stainless steel and (b) 316 L stainless steel with deposited siloxane coating.

Fig. 3(a–b) presents the EDS analysis results of the bare and siloxane–modified steel surfaces as additional proof of the presence of the siloxane coating on the steel surface. The bands corresponding to the iron (ca. 0.7 (L_α), 6.4 (K_α) and 7.1 (K_β) keV), chromium (ca. 0.6 (L_α), 5.4 (K_α) and 5.9 (K_β) keV), nickel (ca. 0.7 (L_α), 7.5 (K_α) and 8.3 (K_β) keV), molybdenum (ca. 2.3 (L_α and L_β) keV) and oxygen (ca. 0.5 (K_α) keV) clearly indicate that the unmodified surface is covered with a thin, passive oxide film (Fig. 3(a)) [6]. There are also peaks corresponding to silicon (ca. 1.7 (K_α) keV) and manganese (ca. 0.6 (L_α) and 5.9 (K_α) keV), which are alloying elements of this type of steel. In the case of a modified sample, it is obvious that the enormous increase in the peak intensity for silicon is caused by the siloxane coating deposition (Fig. 3(b)). This deposition is accompanied by a huge decrease in the intensity of the peaks for iron, chromium, nickel and molybdenum when compared to the unmodified sample. In addition, the increase in the intensity of the oxygen is interesting, as well as the carbon (ca. 0.3 (K_α) keV) peaks, which also indicate that a siloxane coating containing siloxane bonds, alkyl chain, hydroxyl and alkoxy moieties is prevalent on the surface of the so-modified oxide layer.

3.2. Electrochemical measurements

The results of the electrochemical tests confirm the previous assumptions and conclusions drawn on the basis of the physicochemical analysis. Fig. 4(a) shows the OCP of samples 316 L/28 and

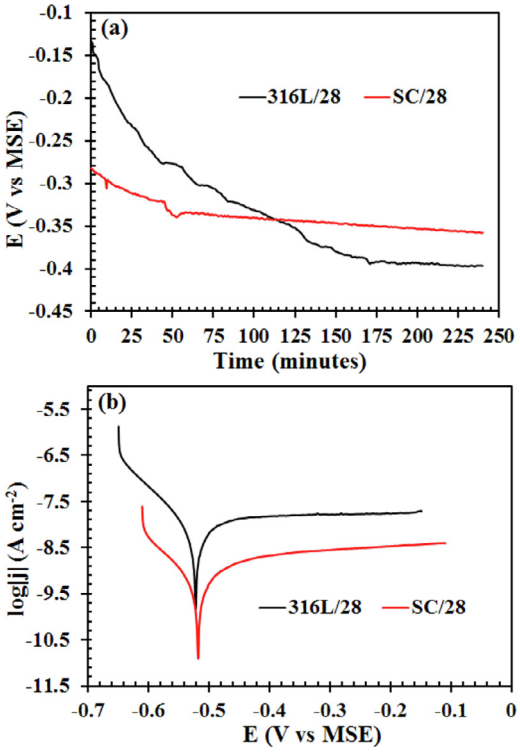

Fig. 4. (a) Open circuit potential (OCP) versus time and (b) potentiodynamic polarization (PP) curves of all tested samples (316 L/28 and SC/28). Measurements were performed in a 1 M Na_2SO_4 solution at ambient conditions.

SC/28. It can be stated that the 316 L stainless steel with the deposited siloxane coating has a higher, more noble OCP compared to the bare 316 L stainless steel surface. In the initial phase of the test, the potential of the bare steel is the highest; however, with the elapsed time, it is systematically decreasing. This decrease is most likely caused by the dissolution of the passive oxide film surface and penetration of this layer by electrolyte ions [43-47]. As already mentioned, the metal ions, which are the components of steel, pass into the electrolytic solution [6]. As previously demonstrated, the siloxane coating deposited from an aqueous solution (SC/28) is porous. Therefore, during the test, the potential decreases. This decrease is caused by the soaking of the coating with the electrolyte solution; because of that, the conductive pathways are formed inside the pores. Despite the fact that the initial potential of the SC/28 samples was lower than the potential of 316 L/28, after 4 h of testing in salt, the hydrophobic siloxane coating shows the best anti–corrosive properties. This outcome is confirmed by the results of the potentiodynamic polarization tests (Fig. 4(b)) and the data contained in Table 2. The values of the corrosion potentials (E_{corr}), corrosion current densities (j_{corr}), slopes of the anodic (β_a) and cathodic (β_k) polarization curves and the corrosion rates (CR) have been determined using the EC–Lab® Software. The best anti–corrosive properties are shown by the sample SC/28. The coating deposited on the SC/28 sample is thicker than the passive oxide film on the steel surface. This fact is demonstrated by the slope of the cathodic curve, which is higher than in the case of 316 L/28.

It has already been stated [6,50,51,76] that in the case of the stainless steel and the stainless steel with deposited siloxane coatings, the thickness of the passive oxide film or siloxane coating affects the slope of the cathodic curve and is responsible for the reduction reactions of the protons or oxygen molecules. For the anodic process, the SC/28 sample has a lower slope. The dissolution process of the oxide layer proceeds much faster in the case of bare steel. For this reason, a thicker layer of ions and prod-

Table 2
Corrosion potentials (E_{corr}), corrosion current densities (j_{corr}), and slopes (β_a and β_c) of the polarization curves and corrosion rates (CR) of all the tested samples (316 L/28 and SC/28), as determined by the EC–Lab® Software.

Sample	E_{corr} (mV vs MSE)	j_{corr} (nA ·cm^{-2})	β_a (mV)	$-\beta_c$ (mV)	CR•10^{-3} (mm·y^{-1})
316 L/28	–522	14.3	2632	98	0.162
SC/28	–518	1.6	814	147	0.016

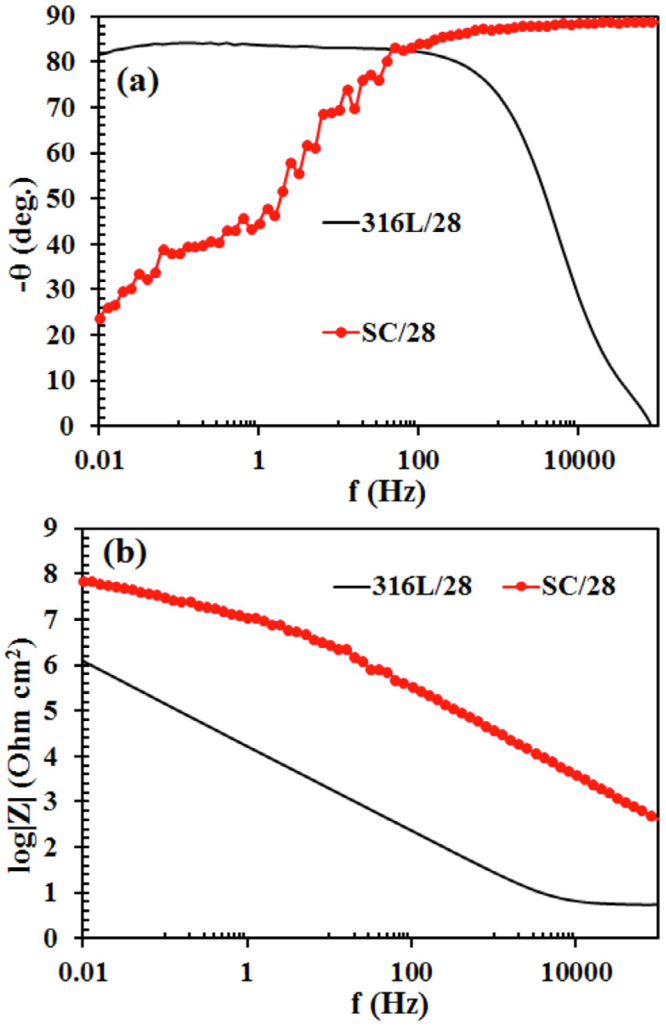

Fig. 5. Bode plots of 316 L/28 and SC/28 samples: (a) phase angle vs frequency and (b) impedance modulus vs frequency.

ucts is formed at the oxide/electrolyte interface than in the case of the steel covered with a siloxane coating that is additionally soaked with electrolyte solution. The determined corrosion potentials of the 316 L/28 and SC/28 samples confirm that the second one shows the best anti–corrosive properties. However, in this case, the difference between the two samples is not as pronounced as in the case of the corrosion current density. Due to the presence of a coating, the corrosion process of steel is more than eight times slower. The value of the corrosion current density is equal to 1.6 nA·cm^{-2}. The results of the potentiostatic electrochemical impedance spectroscopy (PEIS) measurements confirm the above assumptions. Fig. 5(a–b) shows the Bode plots of all the samples. In the high frequency range, the phase angle (θ) is the lowest in the case of the SC/28 sample (Fig. 5(a)). This outcome confirms the hypothesis that there is a thick and uniform hydrophobic coating on the surface. The value of the phase angle in the high frequency range is in this case almost equal to –90° Thus, the coating behaves similar to an almost ideal capacitor [77,78]. The thickness and/or uniformity of the coating with hydrophobic properties, which is located on the surface of 316 L stainless steel, directly affects the value of its effective capacitance, i.e., as the thickness and/or uniformity increases, the effective capacitance decreases [76-80]. The highest θ is found for the bare, unmodified 316 L stainless steel surface with only the passive oxide film. As mentioned before, this layer is much thinner than the siloxane layers. The phase angle decreases in the whole frequency range. This decrease is an indication of the dissolution of the passive oxide film, which in the electrolyte solution is built up with a layer of oxides, hydroxides, oxohydroxides and salts that are the products of steel corrosion.

In the middle frequency range, the phase angle of the SC/28 sample continually increases. In this case, the curve in the range from 100 kHz to approximately 1 Hz is a reflection of the presence of the siloxane coating. In the range of low frequencies (below 1 Hz), a second time constant that is responsible for the electrolyte/passive oxide film interface formation starts to appear.

As mentioned before, the deposited coating is porous. This characteristic impacts the contact between the electrolyte and the surface of the passive oxide film. In the low frequency range, a soft *plateau* appears (SC/28). After a certain time, θ starts to increase again. In the case of bare steel, the curve shown in Fig. 5(a) corresponds to one time constant referring to the electrical double–layer at the electrolyte/passive oxide film interface [52,81,82].

Fig. 5(b) shows a dependency between the impedance modulus and the frequency of the applied signal. In the range of high frequency values, a *plateau* (316 L stainless steel) appears. Such behaviour corresponds to the equivalent series resistance of the solution and various types of electrical connections in the test cell. In the case of SC/28, this *plateau* is missing in the given frequency range due to the presence of the siloxane coating. However, it does not mean that the presence of a resistance element in this case should be excluded. Simply, for such a thick coating, the *plateau* might appear in the range of even higher frequency values. In the range of middle frequency values, a straight line with a slope of (–1) appears, and it is affected by the presence of a slightly pronounced *plateau*. This presence, in turn, reflects the resistance of the coating and the resistance of the electrochemical reactions. When comparing the two graphs, i.e., the diagrams of the phase angle and impedance module versus frequency, the decrease in the phase angle values (Fig. 5(a)) is related to the straight line with a slope (–1) (Fig. 5(b)), while the increase is associated with the presence of a *plateau* in Fig. 5(b).

Fig. 6(a–d) shows the Nyquist plots of the 316 L stainless steel and SC/28. The solid lines indicate the data which were fitted to the obtained experimental results (symbols). On this basis, the equivalent electrical circuits (EEC) were selected (Fig. 6(a–b)). They contain two different time constants, i.e., Q_{dl}/R_{ct} and Q_c/R_cM, Q_{dl}/R_{ct}, in which the constant phase element parameter Q and the resistor R with the diffusion element showing a special diffusion case, i.e., the restricted linear diffusion M (SC/28), are connected in parallel. The constant phase element (CPE) expresses the non–ideal capacitance of a given system. It is a reflection of the non–ideal ca-

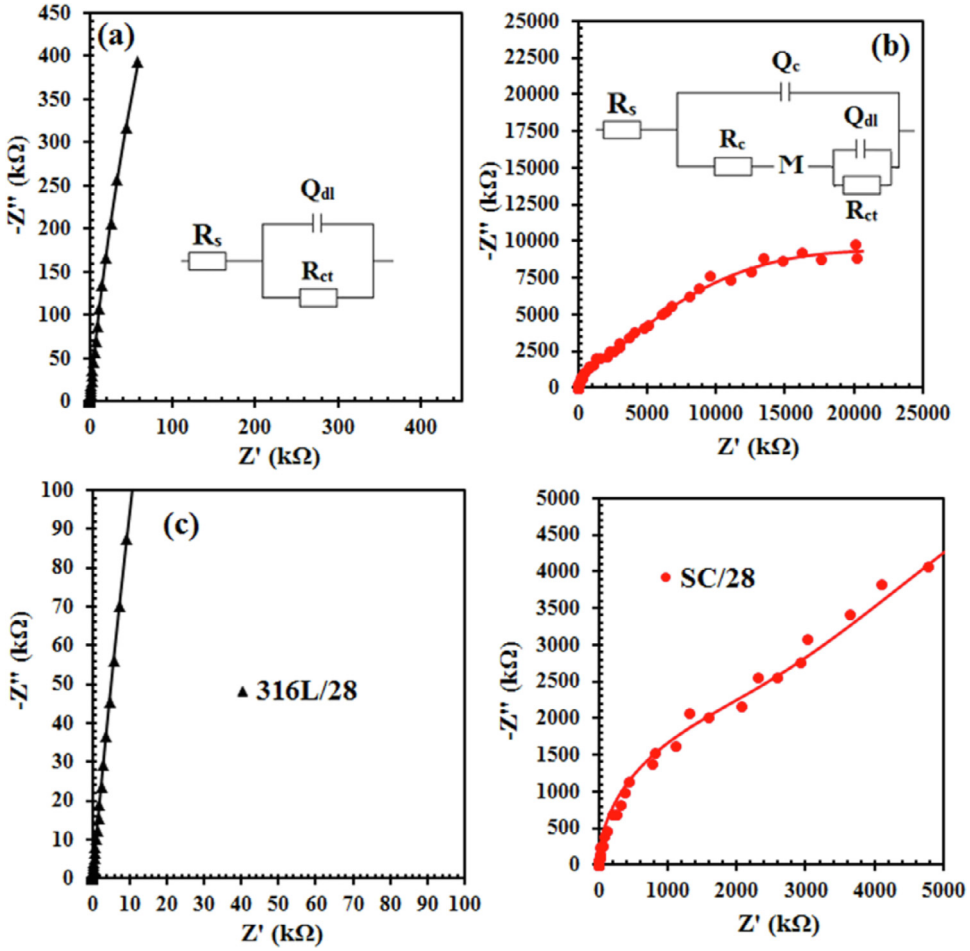

Fig. 6. (a–d) Nyquist plots of the 316 L/28 and SC/28 tested samples. Equivalent electrical circuits used for fitting the PEIS data of the 316 L stainless steel and SC/28 sample. Measured data (symbols) and fitted data (solid lines). (For interpretation of the references to colour in this figure legend, the reader is referred to the web version of this article.)

pacitor. The CPE impedance is given by the following:

$$Z_{CPE}(j\omega) = \frac{1}{Q(j\omega)^{\alpha}} \quad (1)$$

where j is the imaginary number, ω is the angular frequency and α is the factor reflecting the capacitive dispersion. If the exponential factor α is lower than unity ($\alpha<1$), the parameter Q does not express the capacitance. Therefore, it should be provided as $F{\cdot}s^{(\alpha-1)}$ [76,79,80]. The R_s element is an equivalent series resistance (ESR) of the electrolyte solution and various types of electrical connections of the cell system. The circuit shown in Fig. 6(a) presents the constant phase element parameter of the electrical double–layer (Q_{dl}), which is formed at the electrolyte/passive oxide film interface, and the charge transfer resistance (R_{ct}) between these two phases. Barsoukov and MacDonald [78] suggest that the equivalent electrical circuit for impedance testing of metal and steel systems with the passive oxide layer in the aqueous electrolyte solution should contain three time constants. According to the authors, these are constants describing the passive oxide film and two interfaces, i.e., the electrolyte/passive oxide film and the passive oxide film/metal (or steel). Kocijan et al. [81] suggest the possibility of choosing four different equivalent electrical circuits for stainless steel immersed in an aqueous electrolyte. These circuits contain one or two time constants that describe the passive oxide film as well as the electrical double–layer and the charge transfer resistance. The Nyquist curve for 316 L stainless steel (Fig. 6(a, c)), which contained a passive oxide film, represents one loop (poorly developed semicircle), i.e., one time constant. Therefore, EEC with Q_{dl} and R_{ct} elements (Fig. 6(a)) was chosen for the 316 L stainless steel sample, while for the sample with siloxane coating, the EEC shown in Fig. 6(b) was chosen.

The second circuit (Fig. 6(b)) contains the constant phase element parameters expressing the non–ideal capacitance (Q_c) and resistance (R_c) of the siloxane coating, as well as non–ideal capacitance (Q_{dl}) and charge transfer resistance (R_{ct}) concerning the electrical double–layer at the electrolyte/passive oxide film interface. As has been mentioned, the porous siloxane coating is soaked with electrolyte solution; hence, conductive pathways are formed in its structure. Additionally, there is also a presence of diffusion element M, which describes a special diffusion phenomenon. It is assumed that this is a diffusion of mass (ions, oxides, hydroxides, oxyhydroxides and salts) through the porous siloxane coating and mainly under the coating, i.e., on the passive oxide film surface [76]. In the case of siloxane coatings deposited on the surface of the stainless steel oxide layer, the amount and type of corrosion products formed under the coating (on the surface of the passive film [59]) determine the occurrence of the restricted linear diffusion phenomena with reflective boundary conditions. Passive oxide film builds up with a layer of oxides and hydroxides. In addition, in the vicinity of this layer, there is an electrolyte solution, which is also rich in the above–mentioned corrosion products, and additional ions (also steel components). The phenomenon of restricted linear diffusion with reflective boundary conditions should be precisely characteristic of this moment of the PEIS test execution (af-

Table 3
The values of all the individual components of all the equivalent electrical circuits from Fig. 5(a–b), as determined by the EC–Lab® Software.

Sample	$Q_c \cdot 10^{-9}$ (F $s^{(\alpha-1)}$)	R_c (kΩ)	R_d (Ω)	$Q_{dl} \cdot 10^{-6}$ (F $s^{(\alpha-1)}$)	R_{ct} (kΩ)
316 L/28	–	–	–	33.8	7055
SC/28	17.7	2863	154,890	0.13	29,190

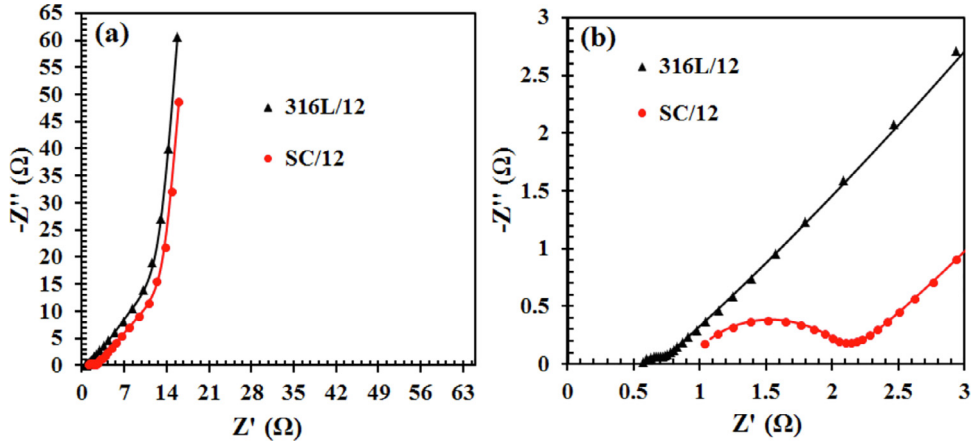

Fig. 7. (a–b) Nyquist plots of electrochemical capacitors 316 L/12 and SC/12. The measurements were performed with the Swagelok® cell assembly. Measured data (symbols) and fitted data (solid lines). The selected curves represent two–electrode cell measurements. (For interpretation of the references to colour in this figure legend, the reader is referred to the web version of this article.)

ter 4 h) in an aqueous electrolyte solution for the so–modified steel surface. This is also confirmed by our previous publication [76]. Equation (2) presents the impedance of the restricted linear diffusion element (reflective boundary conditions), as follows [1,77,78,83-85]:

$$Z_M(j\omega) = R_d \frac{\coth(\sqrt{\tau_d j\omega})}{\sqrt{\tau_d j\omega}}$$

where R_d represents diffusion resistance, τ_d is the diffusion time constant, which is equal to the quotient of L^2/D, where L is a diffusion layer thickness, while D is the diffusion coefficient.

Table 3 shows the constant phase element parameter and resistance values of each individual component of all the equivalent electrical circuits from Fig 6(a–b), as determined by the EC–Lab® Software. It is obvious that a thicker siloxane coating is a better insulator than the electric double layer. Thus, the value of Q_c is much lower than that of Q_{dl}. The same applies to the charge transfer resistance R_{ct}. In the case of the sample with siloxane coating (SC28), this value is much higher. The elements describing the siloxane coating have a diametric impact on the values of the second time constant elements related to the electrolyte/passive oxide film interface. Due to the presence of the siloxane coating, the values of Q_{dl} and R_{ct} are incomparably lower and higher, respectively, in comparison to bare, unmodified 316 L stainless steel (316 L/28) [52,81,82].

Fig. 7 shows the Nyquist plots of the electrochemical capacitors in which bare current collectors and those with siloxane coatings were used. The PEIS study was carried out in a two–electrode system as soon as they were constructed. The equivalent electrical circuit (EEC) was matched to the obtained results. The symbols in Fig. 7 show the experimental data, while the lines show the data obtained during the circuit fitting. Fig. 8 shows the EEC, which was adopted for the obtained experimental data of two different electrochemical capacitors, i.e., containing unmodified (316 L/12) as well as modified current collectors (SC/12). The system was adopted for all the obtained PEIS results of all the electrochemical capacitors. Depending on the research stage, i.e., the moment

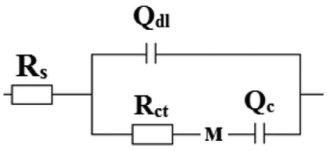

Fig. 8. Equivalent electrical circuit used for fitting the PEIS data of electrochemical capacitors with both types of current collectors, i.e., with (SC/12) and without (316 L/12) deposited siloxane coatings.

at which the PEIS test was carried out, only the values describing the elements of the presented circuit change. All this will be described and analysed below. The elements of the circuit are as follows: R_s – equivalent series resistance, responsible for the resistance of the electrolyte solution and various types of electrical connections in the tested systems; Q_{dl} – constant phase element parameter, describing the electrical double–layer that forms at the electrode/electrolyte interface; R_{ct} – resistor describing the resistance associated with the charge transfer through the electrode/electrolyte interface; M – diffusion element showing a special diffusion case, i.e., restricted linear diffusion with reflective boundary conditions; Q_c – constant phase element parameter describing the non–ideal capacitance of an electrochemical capacitor, which does not depend on the frequency of the given signal [1,14,77,78]. The use of this element instead of the usual capacitor is much more constructive due to the greater accuracy of matching the circuit to the obtained results. The Q_{dl} element corresponds to the non–ideal capacitance of the electrical double–layer at the electrode/electrolyte interface in the high frequency range, i.e., when the applied signal responses vary depending on the frequency. In the range of low frequency values, when the signal is capable of penetrating deeper into the porous carbon electrode, the Q values of the electrical double–layer no longer depend on the frequency of the signal and should be more or less constant [1]. This is described by the constant phase element parameter Q_c. In the case of electrochemical capacitors, the diffusion phenomena play a very important role. This role is clearly visible on the

Table 4
The values of all the individual components of the equivalent electrical circuit from Fig. 7, as determined by the EC–Lab® Software. The presented data refer to the curves depicted in Fig. 6.

Sample	$Q_{dl} \cdot 10^{-3}$ ($F \cdot s^{(\alpha-1)}$)	R_{ct} (Ω)	R_d (Ω)	Q_c ($F \cdot s^{(\alpha-1)}$)
316 L/12	0.13	0.12	33.20	0.41
SC/12	0.22	1.19	31.05	0.58

Nyquist plots. In the range of middle frequency values, there is usually a straight line with a slope (–1). This slope is a reflection of the mass transport to or from the surface of the porous electrode material. In the case when this straight line is between the semicircle (high frequency values) and the vertical straight line (low frequency values), the system is dominated by restricted linear diffusion with reflective boundary conditions. Throughout the test, in the range from high to low frequency values, a semicircle first appears, which corresponds to charging the electrical double–layer, then mass diffusion occurs and finally a straight line appears, also indicating the charging of the electrical double–layer [1,14,77,78].

Table 4 shows the values of the EEC elements fitted to the PEIS results of the electrochemical capacitors as soon as the systems are assembled. Fig. 7 and Table 4 clearly indicate the high impact of the diffusion phenomena on the parameters of the supercapacitors. As mentioned before, the test was carried out under open circuit conditions before the electrodes were widely polarized. For this reason, the electrical double–layer is not saturated with electrolyte solution ions, which are just starting to move. Therefore, mass diffusion dominates in such a system. Comparing both electrochemical capacitors, i.e., containing modified (SC/12) and unmodified (316 L/12) current collectors, it is stated that while the diffusion resistance R_d is of the same value, the charge transfer resistance is much greater in the case of the SC/12 current collectors. This greater resistance is the result of the presence of an additional interface, which in this case, is the siloxane coating.

Fig. 9(a–b) and Fig. 10 show the cyclic voltammograms of two– and three–electrode systems at three different scan rates, i.e., 5 $mV \cdot s^{-1}$ (Fig. 10), 10 $mV \cdot s^{-1}$ (Fig. 9(a)) and 100 $mV \cdot s^{-1}$ (Fig. 9(b)). Higher capacitance values were obtained for a supercapacitor containing unmodified current collectors (316 L/12). In addition, the voltammogram for the 316 L/12 electrochemical capacitor at the scan rate of 100 $mV \cdot s^{-1}$ is characterized by better a charge transfer; i.e., the shape is much closer to rectangular shape than in the case of the modified current collectors (SC/12). This outcome is again the result of the existence of an additional interface, i.e., siloxane coating, the purpose of which is to protect the collector surface against the destructive effect of electrochemical corrosion. On the basis of the potentiodynamic polarization tests (Fig. 4(b) and Table 2), it was found that the value of the corrosion current density of the steel with the coating is much lower than in the case of unmodified steel. This phenomenon also translates directly into the electrochemical characteristics of the supercapacitor, including the potentiostatic electrochemical impedance spectroscopy, cyclic voltammetry, and galvanostatic charging/discharging results, which are additionally provided in the supporting information (Fig. S1). The galvanostatic method indicates longer charging and discharging times of the 316 L/12 electrochemical capacitor. Consequently, it translates into a higher capacitance of the system. This higher capacitance is also confirmed by the galvanostatic cycling measurements (Fig. 11). After 5 000 cycles of galvanostatic charging/discharging of the electrochemical capacitors, the specific capacitance values decrease slightly when compared to the initial values (i.e., before the test). In addition, the difference in the working parameters of both systems remains unchanged, i.e., the cycling test does not affect in any way the nature of the processes occurring at the interfaces. The supporting information section (Fig. S2(a–d), S3(a–b) and S4(a–d)) presents the PEIS results (Nyquist curves) of the electrochemical capacitors after 25, 50, 75, 100, 125, 150, 175 and 200 h of floating (voltage–holding test), i.e., after 5, 10, 15, 20, 25, 30, 35 and 40 test cycles. It is worth recalling that between 10 and 11 and 20 and 21 cycles, the tested systems were left at open circuit conditions (24 h).

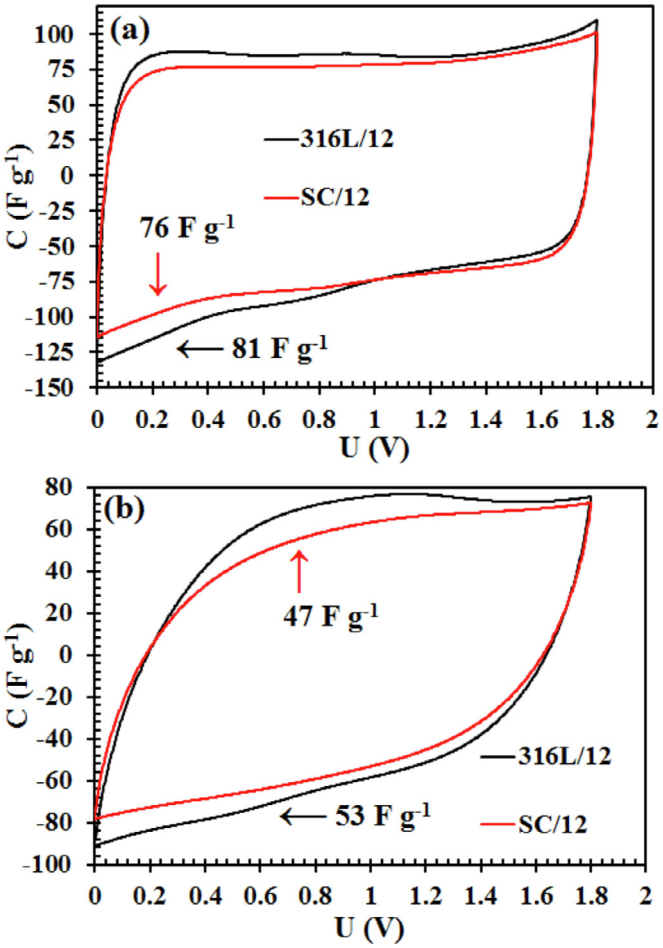

Fig. 9. Cyclic voltammograms of samples 316 L/12 and SC/12. Scan rates: (a) 10 $mV \cdot s^{-1}$ and (b) 100 $mV \cdot s^{-1}$ in two–electrode Swagelok® cells.

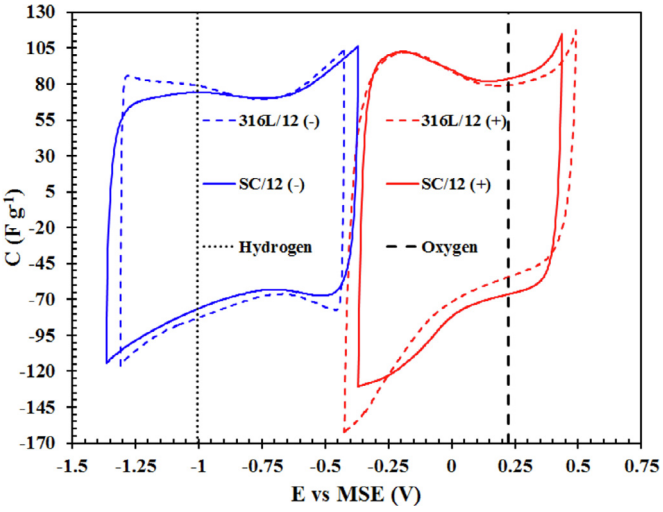

Fig. 10. Cyclic voltammograms of samples 316 L/12 and SC/12. Scan rate: 5 $mV \cdot s^{-1}$ in three–electrode Swagelok® cells.

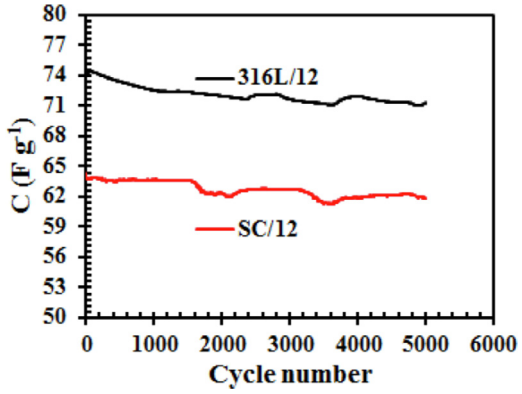

Fig. 11. Specific capacitance derived from the galvanostatic charging/discharging cyclic tests. Current density: 2 $A \cdot g^{-1}$. Two–electrode Swagelok® cell.

Table 5
The values of all the individual components of the equivalent electrical circuit from Fig. 7, as determined by the EC–Lab® Software. The PEIS results were derived after 25 h and 50 h of floating.

Sample	$Q_{dl} \cdot 10^{-3}$ ($F \cdot s^{(\alpha-1)}$)	R_{ct} (Ω)	R_d (Ω)	Q_c ($F \cdot s^{(\alpha-1)}$)
25 h				
316 L/12	4.16	0.99	2.77	1.43
SC/12	0.11	2.34	2.95	0.55
50 h				
316 L/12	4.72	1.25	2.94	0.99
SC/12	0.11	2.16	2.77	0.52

Table 6
The values of all the individual components of the equivalent electrical circuit from Fig. 7, as determined by the EC–Lab® Software. The PEIS results were derived after 75 h and 100 h of floating.

Sample	$Q_{dl} \cdot 10^{-3}$ ($F \cdot s^{(\alpha-1)}$)	R_{ct} (Ω)	R_d (Ω)	Q_c ($F \cdot s^{(\alpha-1)}$)
75 h				
316 L/12	3.94	1.95	3.79	0.61
SC/12	0.09	3.96	2.40	0.51
100 h				
316 L/12	1.53	2.43	3.86	0.24
SC/12	0.09	4.49	2.54	0.48

Table 7
The values of all the individual components of the equivalent electrical circuit from Fig. 7, as determined by the EC–Lab® Software. The PEIS results were derived after 125 h and 150 h of floating.

Sample	$Q_{dl} \cdot 10^{-3}$ ($F \cdot s^{(\alpha-1)}$)	R_{ct} (Ω)	R_d (Ω)	Q_c ($F \cdot s^{(\alpha-1)}$)
125 h				
316 L/12	0.48	2.15	2.54	0.13
SC/12	0.10	3.55	2.63	0.81
150 h				
316 L/12	0.53	3.16	5.89	0.07
SC/12	0.09	4.02	3.32	0.51

The EEC shown in Fig. 8 is the most suitable, best fitted circuit for all of the obtained PEIS results, including even those performed during the long–term ageing procedure. Tables 5, 6, 7 and 8 contain the values of all individual elements of the considered equivalent electrical circuits, depending on the stage of the measurements, i.e., from 25 to 200 h of floating (from 5 to 40 cycles). Based on the obtained results, it can be stated that in the case of a supercapacitor with unmodified current collectors, the charge transfer resistance (R_{ct}) increases with the time, i.e., as the number of cycles increases. While the changes in R_{ct} in this case are not very pronounced, the increase in the resistance value resulting from the diffusion processes (R_d) is enormous, especially after 175 h of floating (215.4 Ω). It is important to note that the upward

Table 8
The values of all the individual components of the equivalent electrical circuit from Fig. 7, as determined by the EC–Lab® Software. The PEIS results were derived after 175 h and 200 h of floating.

Sample	$Q_{dl} \cdot 10^{-3}$ ($F \cdot s^{(\alpha-1)}$)	R_{ct} (Ω)	R_d (Ω)	Q_c ($F \cdot s^{(\alpha-1)}$)
175 h				
316 L/12	3.23	9.96	215.40	0.03
SC/12	0.03	26.82	1.67	0.09
200 h				
316 L/12	–	–	–	–
SC/12	0.04	18.34	0.52	0.09

trend in the R_{ct} and R_d (316 L/12) values changes in only one situation; i.e., these values are greater after 100 h than after 125 h. This outcome is most likely caused by the relaxation time (24 h) between the cycles 20 and 21. The Nyquist curve, after 200 h of floating, has a shape that clearly indicates the destruction of the supercapacitor. No EEC has been selected for this curve. Most likely, the major role in this case is the diffusion phenomena of the steel corrosion products. Considering the constant phase element parameter Q_c value, a clear decrease along with the duration of the floating is noticed. However, in regard to changes in the value of an element describing the formation of an electrical double–layer in the range of high frequency values (Q_{dl}), there is no reasonable correlation. In the case of supercapacitors with siloxane coatings deposited on the surface of the current collectors (SC/12), the same trend is observed, i.e., the increase of the charge transfer resistance (R_{ct}) up to 20 cycles, followed by a decrease and then another increase. The only difference is that R_{ct} starts to decrease again after the 40th cycle. The diffusion resistance (R_d) oscillates between 2.40 and 3.32 Ω. After the 35th cycle, i.e., after 175 h of floating, it decreases. During the second series of tests, i.e., after 100 h of floating, the Q_c value of the SC/12 electrochemical capacitor decreased. After 24 h of relaxation under open circuit conditions, it increased and from that point, it started to decrease again. The value of the Q_{dl} remained at approximately the same level during the 200 h of floating. When comparing two types of electrochemical capacitors such as 316 L/12 and SC/12, it should be noted that the first of them, until the end of the second series (100 h), had a higher Q_c value. Fig. 12(a–d) and 13(a–d) show the comparison of the Nyquist curves of the two types of supercapacitors in the individual stages of the long–term ageing procedure.

Fig. 14 depicts the cyclic voltammetry results, which were carried out exactly one week after the end of the floating. At that time, the systems were not polarized. The presented curves clearly confirm the fact that only the electrochemical capacitor with unprotected current collectors was destroyed. The capacitance has been reduced. The confirmation of the above observation is also the result of three–electrode measurements (Fig. 15(a–d) and S5(a–d)). Fig. S6(a–b), S7(a–b) and S8 represent a comparison of the individual test system results before and after a long–term ageing procedure. On this basis, it is clear that in the case of an electrochemical capacitor containing current collectors 316 L/12, the positive electrode is responsible for the degradation of the performance [6,43-47]. This electrode undergoes oxidation reactions during the charging mode. According to Barsoukov and Macdonald [78], the growth and breakdown of the passive oxide film could be described by the point defect model, i.e., in such a film, there is an (i) electronic current due to the transport of electrons and electron holes, and (ii) an ionic current due to the transport of anion and cation vacancies. Passive oxide film consists of two layers, i.e., a barrier layer, which is situated on the metal or steel surface, and an outer layer, which is adjacent to the electrolyte solution. The latter is more porous and consists not only of oxides but also hydroxides, oxyhydroxides and metal salt compounds. Ad-

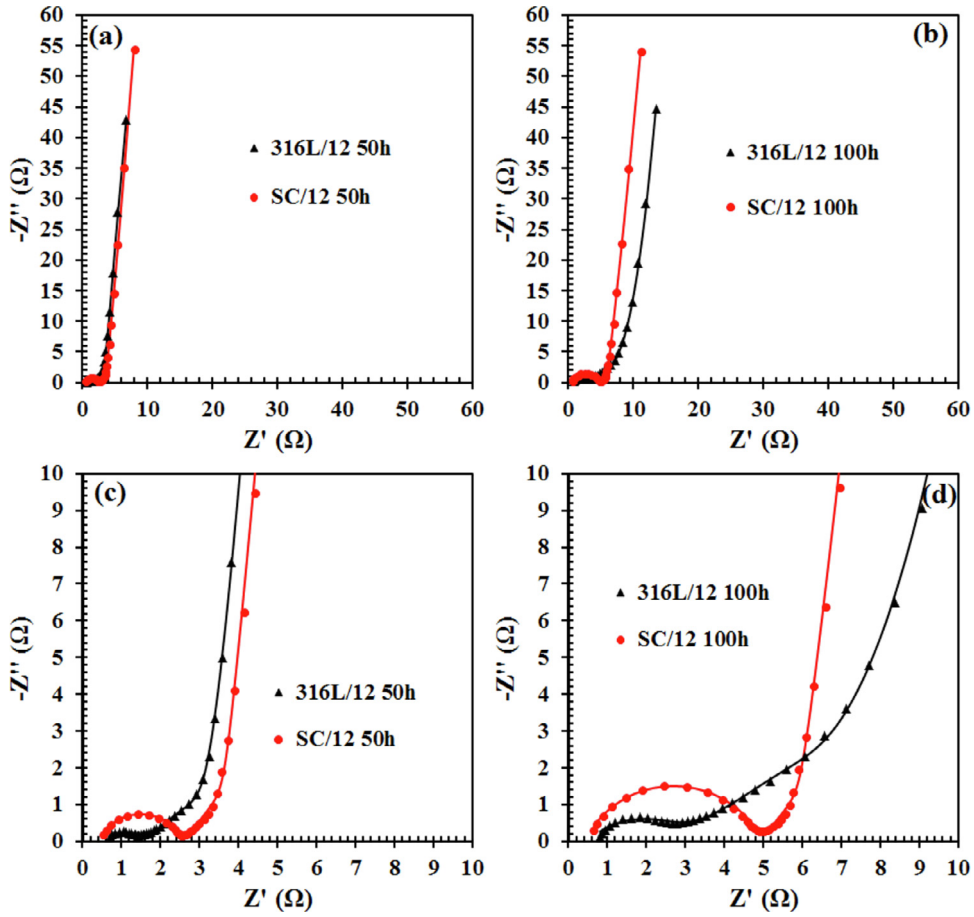

Fig. 12. (a–d) Comparison of the Nyquist plots of electrochemical capacitors 316 L/12 and SC/12, which were subjected to floating tests. The selected curves represent measurements performed after 50 h and 100 h of floating. Measured (symbols) and fitted data (solid lines). Two–electrode Swagelok® cell. (For interpretation of the references to colour in this figure legend, the reader is referred to the web version of this article.)

ditionally, it is filled with an electrolyte solution. Defects in the structure of the oxide film arise and are annihilated at the same time. Briefly, it is related to the movement of cation vacancies from the outer/barrier layers towards the steel/barrier layer interfaces and oxygen vacancies in the opposite direction. As a result, cations are transferred from the steel to the passive oxide film (barrier layer), while the electrolyte solution remains a source of oxygen atoms. With regard to the phenomenon of anodic polarization of steel, i.e., extremely strong polarization in the electrochemical capacitors (positive electrode), which operate in the voltage range of 1.8 V, the phenomenon of steel transpassivation should be taken into account. It is a transfer of metal cations from the structure of the barrier layer and dissolution of the passive oxide film. As mentioned before, in contrast to the barrier layer, the outer one is filled with electrolyte solution and is weakly bonded to the substrate, which is also the essence of the restricted linear diffusion element application (Fig. 6(b) and 8). Certainly, the dissolution of the passive oxide film under the siloxane coating takes place, but due to the coating hydrophobicity, it is a slower process than in the case of the unmodified surface. Therefore, the current collector, which is in constant contact not only with the electrode material but also with the electrolyte solution, most likely dissolves. The components of the 316 L stainless steel pass into electrolyte in the form of ions and various types of compounds. In addition, oxidation reaction products are formed on the surface of the unmodified current collector (316 L stainless steel) [6].

In our previous paper [6], we described in detail the effect of the electrolyte solution on the corrosion phenomena of the current collector (316 L stainless steel) and, thus, on the performance of an electrochemical capacitor. By means of physicochemical analysis (atomic force microscopy (AFM), energy–dispersive X–ray spectroscopy (EDS) and Raman spectroscopy) assisted by electrochemical techniques, the probable composition of the resulting passive oxide film in the 1 M Na_2SO_4 electrolyte solution was accurately characterized. In addition, it was found that the pores of the resulting layer are filled with soluble and insoluble metal sulphate compounds. During charging (or more precisely – during floating), the passive oxide film most likely breaks off to some extent and the products transfer into the electrolyte. The resulting products block the access of the electrolyte ions to the porous space of the activated carbon material. This blockage is indicated by the enormous increase in the diffusion resistance (R_d). In addition, the thick oxide, hydroxide, oxohydroxide and salts layer increases the charge transfer resistance through the interfaces. The degradation of the current collector described in this way affects the degradation of the positive electrode, understood as a whole, and consequently leads to a decrease in the capacitance value of an electrochemical capacitor. This degradation is also revealed by the characteristics of PEIS, and more specifically the Nyquist plots of the positive electrode with unmodified current collectors (Fig. 15(a)). The electrochemical characteristics of supercapacitors with siloxane coated current collectors are completely different. After performing a long–term ageing procedure, none of the electrodes were destroyed.

This outcome is confirmed by both two– and three–electrode measurements (Fig. 14, 15(a–d), S5(a–d)). Additionally, the capac-

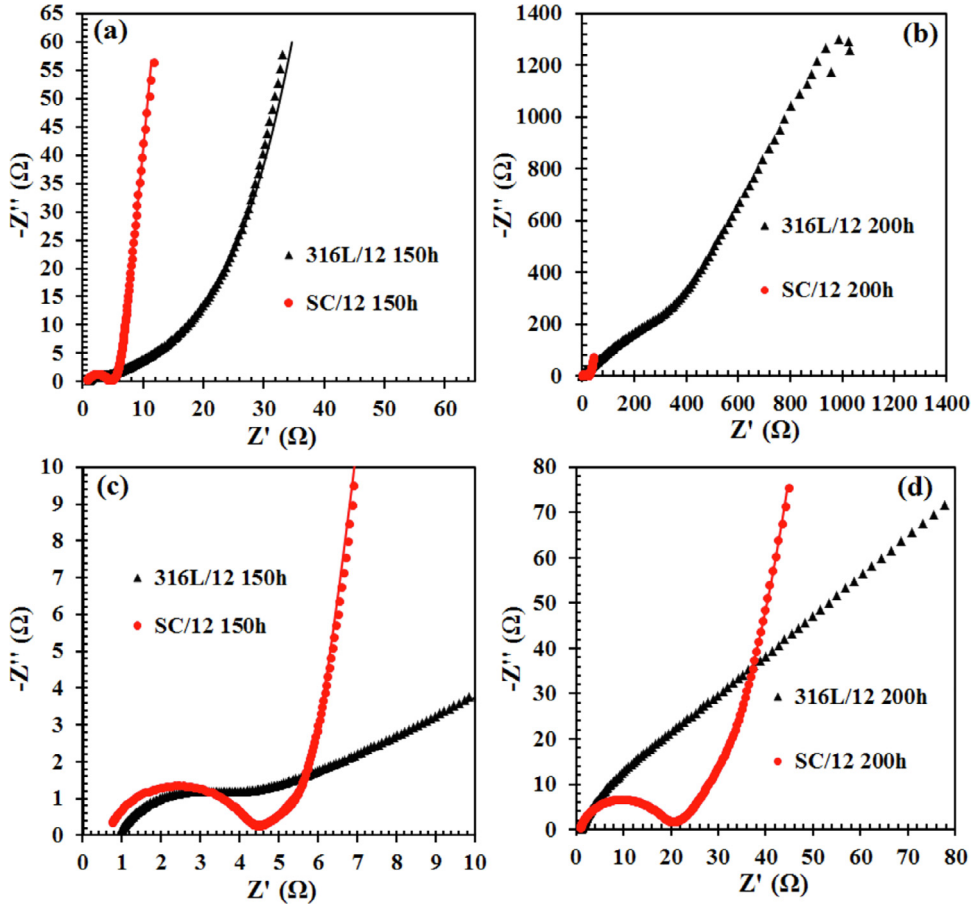

Fig. 13. (a–d) Comparison of the Nyquist plots of electrochemical capacitors 316 L/12 and SC/12, which were subjected to floating tests. The selected curves represent measurements performed after 150 h and 200 h of floating. Measured (symbols) and fitted data (solid lines). Two–electrode Swagelok® cell. (For interpretation of the references to colour in this figure legend, the reader is referred to the web version of this article.)

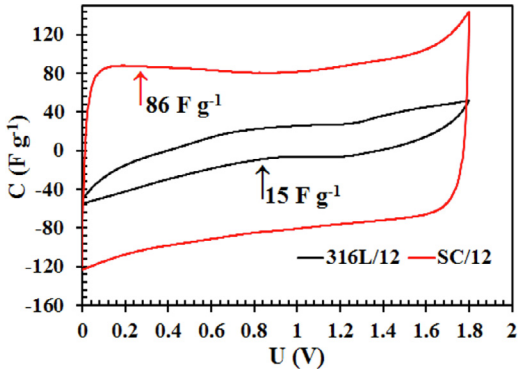

Fig. 14. Comparison of the CV test curves (10 mV s^{-1}) of electrochemical capacitors 316 L/12 and SC/12, which were subjected to floating tests in a two–electrode Swagelok® cell.

itance of the system has increased. During floating, the charge transfer resistance (R_{ct}) has been increasing up to the 40th cycle. After 200 h of floating, the R_{ct} decreased. Siloxane coatings are porous and after a certain time, they are soaked with electrolyte solution, which occurs even faster if the system is polarized. During floating, the electrolyte slowly filled the coating. It is obvious that the mentioned coatings do not form perfect barrier protection, i.e., they do not completely separate the steel surface from the electrolyte environment. Then, from the point of view of use in electrochemical capacitors, it would not make any sense at all. Thus, some of the aggressive ions reach the surface of the passive oxide film, i.e., under the coating, and to a certain extent the corrosion process begins. It should be mentioned that the oxide layer under the siloxane coating is different from that which was formed under corrosive conditions on the surface of the 316 L/12 current collectors, i.e., it is much thinner and less porous. However, a certain part of its surface is degraded. The rest is protected by metal–O–Si bonds [52]. For some reason, the R_{ct} values increase only to a certain point during floating. The diffusion resistance is more or less stable and is low compared to the unmodified supercapacitor (316 L/12). This state is probably caused by the continuous soaking of the coating (low diffusion resistance) and the creation of corrosion products under the coating (increasing R_{ct} values). After some time, the ratio of these two phenomena starts to change; i.e., at some point (40th cycle), the formation of corrosion products under the coating is not as significant as the volume of the electrolyte solution in the coating itself. This outcome causes the decrease in the charge transfer resistance (R_{ct}) after 200 h of floating. One can conclude that the coating, which should be an additional resistor in the tested system, in fact protects this system in the long–term performance from becoming a real resistor. In other words, the introduction of the coating to the system results in the conversion of one resistor to the other. At the beginning of the long–term ageing procedure, the passive oxide film on the 316 L/12 positive current collector showed lower resistance than the interface of the passive oxide film/siloxane coating. However, during floating, the abovementioned layer was covered by corrosion prod-

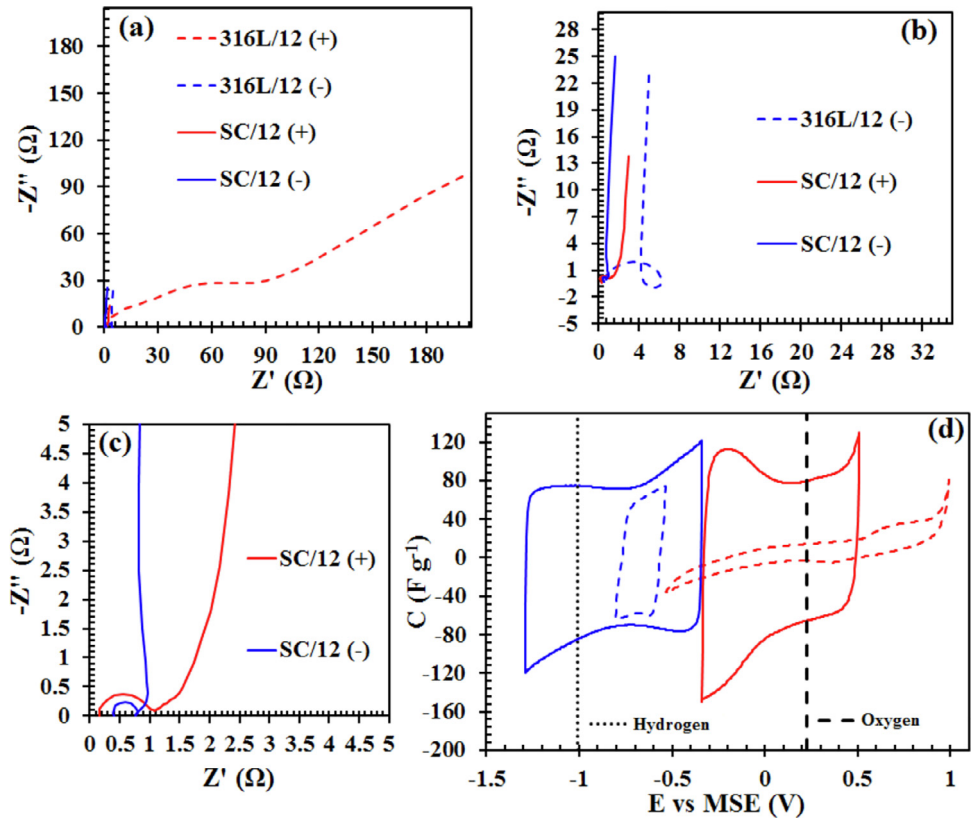

Fig. 15. Comparison of (a–c) Nyquist plots and (d) CV test curves of electrochemical capacitors 316 L/12 and SC/12, which were subjected to floating tests. The selected curves represent three–electrode cell measurements.

ucts, which also pass into the electrolyte solution. This situation prompted the charge transfer and diffusion resistance (R_d) values to increase. In turn, due to the presence of a siloxane coating, R_{ct} increased slightly. In addition, the siloxane coating was constantly soaked in the electrolyte solution, thus creating conductive pathways. The presented research results and conclusions point to an extremely important fact, i.e., of the electrochemical corrosion processes of the current collectors have an extremely important influence on the performance parameters of an electrochemical capacitor. This impact might be much larger (or appear faster) than the contribution from the carbon material degradation.

Conclusions

It is widely known that due to the presence of hydrophobic alkyl chains, siloxane coatings possess anti–corrosive properties; i.e., they protect the surface of metals against the harmful effects of the electrochemical corrosion processes. This protection is also confirmed by the results of the water contact angle, as well as electrochemical technique measurements. Siloxane coatings were chosen to protect the steel from corrosion in electrochemical capacitor systems.

For this purpose, steel current collectors were covered with the same coating, in the same way. During the long–term ageing procedures, which were performed with electrochemical techniques, the supercapacitor with unprotected current collectors was totally damaged. It is assumed that the positive electrode is responsible for this performance decay since it was oxidized during charging. The current collector, which is an element of this electrode, was found to be dissolved. The second system, i.e., containing siloxane coatings, continued to work without any remarkable deterioration.

Based on the obtained results, it is concluded that the corrosion process of current collectors significantly influences the long–term performance of electrochemical capacitors. This influence appears much faster than the degradation of the electrode material and cannot be neglected once long–term performance is evaluated.

Declaration of Competing Interest

None

Acknowledgements

The authors would like to acknowledge the financial support of the National Science Centre of Poland granted on the basis of the decision number DEC–2013/10/E/ST5/00719.

The European Research Council (ERC) is acknowledged for funding provided within the ERC–StG–2017 project (Grant Agreement No. 759603) under the European Union's Horizon 2020 research and innovation programme.

CRediT author statement

All authors declare equal contribution to this work.

Supplementary materials

Supplementary material associated with this article can be found, in the online version, at doi:10.1016/j.electacta.2021.137840.

References

[1] F. Béguin, E. Frąckowiak, Supercapacitors, Wiley-VCH Verlag GmbH & Co. KGaA, Weinheim, Germany, 2013.
[2] B.E. Conway, Electrochemical supercapacitors, 1999.
[3] A. Burke, R&D considerations for the performance and application of electrochemical capacitors, Electrochim. Acta 53 (2007) 1083–1091.

[4] R. Kötz, M. Carlen, Principles and applications of electrochemical capacitors, Electrochim. Acta 45 (2000) 2483–2498.
[5] G. Lota, J. Tyczkowski, P. Makowski, J. Balcerzak, K. Lota, I. Acznik, D. Pezi-ak-Kowalska, L. Kolanowski, The modified activated carbon treated with a low-temperature iodine plasma used as electrode material for electrochemical capacitors, Mater. Lett. 175 (2016) 96–100.
[6] J. Wojciechowski, L. Kolanowski, A. Bund, G. Lota, The influence of current collector corrosion on the performance of electrochemical capacitors, J. Power Sources 368 (2017) 18–29.
[7] M. Gras, L. Kolanowski, J. Wojciechowski, G. Lota, Electrochemical supercapacitor with thiourea-based aqueous electrolyte, Electrochem. Commun. (2018) 32–36.
[8] P. Simon, Y. Gogotsi, Charge storage mechanism in nanoporous carbons and its consequence for electrical double layer capacitors, Philos. Trans. A Math. Phys. Eng. Sci. 368 (2010) 3457–3467.
[9] P. Simon, Y. Gogotsi, Capacitive energy storage in nanostructured carbon-electrolyte systems, Acc. Chem. Res. 46 (2013) 1094–1103.
[10] F. Beguin, V. Presser, A. Balducci, E. Frackowiak, Carbons and electrolytes for advanced supercapacitors, Adv. Mater. 26 (2014) 2219–2251 2283.
[11] P. Simon, Y. Gogotsi, Materials for electrochemical capacitors, Nat. Mater. 7 (2008) 845–854.
[12] Panasonic.
[13] J.R. Miller, A.F. Burke, Electrochemical capacitors: challenges and opportunities for real-world applications, Electrochem. Soc. Interface 17 (2008) 53–57.
[14] P.L. Taberna, P. Simon, J.F. Fauvarque, Electrochemical characteristics and impedance spectroscopy studies of carbon-carbon supercapacitors, J. Electrochem. Soc. 150 (2003) A292.
[15] B.E. Conway, W.G. Pell, T.C. Liu, Diagnostic analyses for mechanisms of self-discharge of electrochemical capacitors and batteries, J. Power Sources 65 (1997) 53–59.
[16] B.W. Ricketts, Ton-That, Self-discharge of carbon-based supercapacitors with organic electrolytes, J. Power Sources 89 (2000) 64–69.
[17] J. Kowal, E. Avaroglu, F. Chamekh, A. S'enfelds, T. Thien, D. Wijaya, D.U. Sauer, Detailed analysis of the self-discharge of supercapacitors, J. Power Sources 196 (2011) 573–579.
[18] H.A. Andreas, Self-Discharge in Electrochemical Capacitors: a Perspective Article, J. Electrochem. Soc. 162 (2015) A5047–A5053.
[19] G. Shul, D. Belanger, Self-discharge of electrochemical capacitors based on soluble or grafted quinone, Phys Chem Chem Phys 18 (2016) 19137–19145.
[20] L. Garcia-Cruz, P. Ratajczak, J. Iniesta, V. Montiel, F. Beguin, Self-discharge of AC/AC electrochemical capacitors in salt aqueous electrolyte, Electrochim. Acta 202 (2016) 66–72.
[21] E. Frackowiak, F. Beguin, Carbon materials for the electrochemical storage of energy in capacitors, Carbon N Y 39 (2001) 937–950.
[22] T. Brousse, D. Bélanger, J.W. Long, To Be or Not To Be Pseudocapacitive? J. Electrochem. Soc. 162 (2015) A5185–A5189.
[23] P. Ratajczak, K. Jurewicz, F. Beguin, Factors contributing to ageing of high voltage carbon/carbon supercapacitors in salt aqueous electrolyte, J. Appl. Electrochem. 44 (2014) 475–480.
[24] P. Ratajczak, K. Jurewicz, P. Skowron, Q. Abbas, F. Beguin, Effect of accelerated ageing on the performance of high voltage carbon/carbon electrochemical capacitors in salt aqueous electrolyte, Electrochim. Acta 130 (2014) 344–350.
[25] M.L. He, K. Fic, E. Frackowiak, P. Novak, E.J. Berg, Ageing phenomena in high--voltage aqueous supercapacitors investigated by in situ gas analysis, Energy Environ. Sci. 9 (2016) 623–633.
[26] Q. Gao, L. Demarconnay, E. Raymundo-Pinero, F. Beguin, Exploring the large voltage range of carbon/carbon supercapacitors in aqueous lithium sulfate electrolyte, Energy Environ. Sci. 5 (2012) 9611–9617.
[27] K. Fic, G. Lota, M. Meller, E. Frackowiak, Novel insight into neutral medium as electrolyte for high-voltage supercapacitors, Energy Environ. Sci. 5 (2012) 5842–5850.
[28] C. Zhong, Y. Deng, W. Hu, J. Qiao, L. Zhang, J. Zhang, A review of electrolyte materials and compositions for electrochemical supercapacitors, Chem. Soc. Rev. 44 (2015) 7484–7539.
[29] C. Zhong, Y. Deng, W. Hu, D. Sun, X. Han, J. Qiao, J. Zhang, Electrolytes for Electrochemical Supercapacitors, CRC Press, New York, 2016.
[30] A. González, E. Goikolea, J.A. Barrena, R. Mysyk, Review on supercapacitors: technologies and materials, 2016.
[31] M. Salanne, Ionic liquids for supercapacitor applications, Top Curr. Chem. (Cham) 375 (2017) 63.
[32] G.Z. Chen, Supercapacitor and supercapattery as emerging electrochemical energy stores, Int. Mater. Rev. 62 (2017) 173–202.
[33] M. Mirzaeian, Q. Abbas, A. Ogwu, P. Hall, M. Goldin, M. Mirzaeian, H.F. Jirandehi, Electrode and electrolyte materials for electrochemical capacitors, Int. J. Hydrog. Energy 42 (2017) 25565–25587.
[34] P. Azaïs, L. Duclaux, P. Florian, D. Massiot, M.-A. Lillo-Rodenas, A. Linares–Solano, J.-P. Peres, C. Jehoulet, F. Béguin, Causes of supercapacitors ageing in organic electrolyte, J. Power Sources 171 (2007) 1046–1053.
[35] O. Bohlen, J. Kowal, D.U. Sauer, Ageing behaviour of electrochemical double layer capacitors - part II. Lifetime simulation model for dynamic applications, J. Power Sources 173 (2007) 626–632.
[36] O. Bohlen, J. Kowal, D.U. Sauer, Ageing behaviour of electrochemical double layer capacitors part I. Experimental study and ageing model, J. Power Sources 172 (2007) 468–475.
[37] A.M. Bittner, M. Zhu, Y. Yang, H.F. Waibel, M. Konuma, U. Starke, C.J. Weber, Ageing of electrochemical double layer capacitors, J. Power Sources 203 (2012) 262–273.
[38] D. Weingarth, A. Foelske-Schmitz, R. Kötz, Cycle versus voltage hold - which is the better stability test for electrochemical double layer capacitors? J. Power Sources (2013).
[39] M. He, K. Fic, E. Frąckowiak, P. Novák, E.J. Berg, Towards more durable electrochemical capacitors by elucidating the ageing mechanisms under different testing procedures, ChemElectroChem 6 (2019) 566–573.
[40] H.S. Ryu, H.J. Ahn, K.W. Kim, J.H. Ahn, J.Y. Lee, E.J. Cairns, Self-discharge of lithium-sulfur cells using stainless-steel current-collectors, J. Power Sources 140 (2005) 365–369.
[41] C. Zhang, A. Yamazaki, J. Murai, J.W. Park, T. Mandai, K. Ueno, K. Dokko, M. Watanabe, Chelate effects in glyme/lithium bis(trifluoromethanesulfonyl)amide solvate ionic liquids, part 2: importance of solvate-structure stability for electrolytes of lithium batteries, J. Phys. Chem. C 118 (2014) 17362–17373.
[42] H.J. Peng, W.T. Xu, L. Zhu, D.W. Wang, J.Q. Huang, X.B. Cheng, Z. Yuan, F. Wei, Q. Zhang, 3D carbonaceous current collectors: the origin of enhanced cycling stability for high-sulfur-loading lithium-sulfur batteries, Adv. Funct. Mater. 26 (2016) 6351–6358.
[43] N. Perez, Electrochemistry and Corrosion Science, Springer, US, 2004.
[44] E. McCafferty, Introduction to Corrosion Science, Springer-Verlag, New York, 2010.
[45] A. Groysman, Corrosion for everybody, Corros. Everybody (2010) 1–368.
[46] R.W. Revie, H.H. Uhlig, Corrosion and Corrosion Control: An Introduction to Corrosion Science and Engineering, John Wiley & Sons, Inc., New York, 2008.
[47] R.W. Revie, Uhlig's Corrosion Handbook, John Wiley & Sons, Inc., New York, 2011.
[48] P. Przygocki, Q. Abbas, P. Babuchowska, F. Beguin, Confinement of iodides in carbon porosity to prevent from positive electrode oxidation in high voltage aqueous hybrid electrochemical capacitors, Carbon N Y 125 (2017) 391–400.
[49] K.L. Mittal, Silanes and Other Coupling Agents, CRC Press, Leiden, 2009.
[50] K. Szubert, J. Wojciechowski, J. Karasiewicz, H. Maciejewski, G. Lota, Corrosion protection of stainless steel by triethoxyoctylsilane and tetraethoxysilane, Int. J. Electrochem. Sc 11 (2016) 8256–8269.
[51] J. Wojciechowski, K. Szubert, R. Peipmann, M. Fritz, U. Schmidt, A. Bund, G. Lota, Anti-corrosive properties of silane coatings deposited on anodised aluminium, Electrochim. Acta 220 (2016) 1–10.
[52] K. Szubert, J. Wojciechowski, J. Karasiewicz, H. Maciejewski, G. Lota, Corrosion-protective coatings based on fluorocarbosilane, Prog. Org. Coat. 123 (2018) 374–383.
[53] F. Beari, M. Brand, P. Jenkner, R. Lehnert, H.J. Metternich, J. Monkiewicz, H.W. Siesler, Organofunctional alkoxysilanes in dilute aqueous solution: new accounts on the dynamic structural mutability, J. Organomet. Chem. 625 (2001) 208–216.
[54] V.H.V. Sarmento, M.G. Schiavetto, P. Hammer, A.V. Benedetti, C.S. Fugivara, P.H. Suegama, S.H. Pulcinelli, C.V. Santilli, Corrosion protection of stainless steel by polysiloxane hybrid coatings prepared using the sol-gel process, Surf. Coat. Tech. 204 (2010) 2689–2701.
[55] M.F. Montemor, M.G.S. Ferreira, Analytical characterisation and corrosion behaviour of bis-aminosilane coatings modified with carbon nanotubes activated with rare-earth salts applied on AZ31 Magnesium alloy, Surf. Coat. Tech. 202 (2008) 4766–4774.
[56] M.E. Montemor, M.G.S. Feffeira, Cerium salt activated nanoparticles as fillers for silane films: evaluation of the corrosion inhibition performance on galvanised steel substrates, Electrochim. Acta 52 (2007) 6976–6987.
[57] M.F. Montemor, R. Pinto, M.G.S. Ferreira, Chemical composition and corrosion protection of silane films modified with CeO_2 nanoparticles, Electrochim. Acta 54 (2009) 5179–5189.
[58] L. Ejenstam, A. Swerin, J.S. Pan, P.M. Claesson, Corrosion protection by hydrophobic silica particle-polydimethylsiloxane composite coatings, Corros. Sci. (2015) 89–97.
[59] D.Q. Zhu, W.J. van Ooij, Corrosion protection of metals by water-based silane mixtures of bis-[*trimethoxysilylpropyl*]amine and vinyltriacetoxysilane, Prog. Org. Coat. 49 (2004) 42–53.
[60] I. Diaz, B. Chico, D. de la Fuente, J. Simancas, J.M. Vega, M. Morcillo, Corrosion resistance of new epoxy-siloxane hybrid coatings. A laboratory study, Prog. Org. Coat. 69 (2010) 278–286.
[61] X.M. Shi, T.A. Nguyen, Z.Y. Suo, J.L. Wu, J. Gong, R. Avci, Electrochemical and mechanical properties of superhydrophobic aluminum substrates modified with nano-silica and fluorosilane, Surf. Coat. Tech. (2012) 3700–3713.
[62] N.N. Voevodin, N.T. Grebasch, W.S. Soto, F.E. Arnold, M.S. Donley, Potentiodynamic evaluation of sol-gel coatings with inorganic inhibitors, Surf. Coat. Tech. 140 (2001) 24–28.
[63] Y. Lu, W.J. Xu, J.L. Song, X. Liu, Y.J. Xing, J. Sun, Preparation of superhydrophobic titanium surfaces via electrochemical etching and fluorosilane modification, Appl. Surf. Sci. 263 (2012) 297–301.
[64] M. Cieślik, K. Engvall, J. Pan, A. Kotarba, Silane–parylene coating for improving corrosion resistance of stainless steel 316L implant material, Corros. Sci. 53 (2011) 296–301.
[65] Y.Q. Yang, L. Liu, J.M. Hu, J.Q. Zhang, C.N. Cao, Improved barrier performance of metal alkoxide-modified methyltrimethoxysilane films, Thin Solid Films 520 (2012) 2052–2059.
[66] M. Xu, D.Q. Zhu, W.J. van Ooij, Corrosion protection of batch galvanized steels by thin silane films with corrosion inhibitors, Silanes Other Coupl. Agents 5 (2009) 219–230.

[67] D.Q. Zhu, W.J. van Ooij, Corrosion protection of AA 2024-T3 by bis-[3-(*triethoxysilyl*)*propyl*]tetrasulfide in sodium chloride solution. Part 2: mechanism for corrosion protection, Corros. Sci. 45 (2003) 2177–2197.
[68] S.G. Chen, Y.C. Cai, C. Zhuang, M.Y. Yu, X.W. Song, Y.P. Zhang, Electrochemical behavior and corrosion protection performance of bis[triethoxysilylpropyl] tetrasulfide silane films modified with TiO2 sol on 304 stainless steel, Appl. Surf. Sci. 331 (2015) 315–326.
[69] A.F. Scott, J.E. Gray-Munro, J.L. Shepherd, Influence of coating bath chemistry on the deposition of 3-mercaptopropyl trimethoxysilane films deposited on magnesium alloy, J. Colloid Interface Sci. 343 (2010) 474–483.
[70] Z.W. Zhu, G.H. Xu, Y. An, C.H. He, Construction of octadecyltrichlorosilane self-assembled monolayer on stainless steel 316L surface, Colloid Surf. A 457 (2014) 408–413.
[71] F. Zucchi, V. Grassi, A. Frignani, G. Trabanelli, Inhibition of copper corrosion by silane coatings, Corros. Sci. 46 (2004) 2853–2865.
[72] R. Kötz, P.W. Ruch, D. Cericola, Aging and failure mode of electrochemical double layer capacitors during accelerated constant load tests, J. Power Sources 195 (2010) 923–928.
[73] C. Iwakura, Y. Fukumoto, H. Inoue, S. Ohashi, S. Kobayashi, H. Tada, M. Abe, Electrochemical characterization of various metal foils as a current collector of positive electrode for rechargeable lithium batteries, J. Power Sources 68 (1997) 301–303.
[74] J.W. Braithwaite, A. Gonzales, G. Nagasubramanian, S.J. Lucero, D.E. Peebles, J.A. Ohlhausen, W.R. Cieslak, Corrosion of lithiuim-ion battery current collectors, J. Electrochem. Soc. 146 (1999) 448–456.
[75] S.T. Myung, Y. Hitoshi, Y.K. Sun, Electrochemical behavior and passivation of current collectors in lithium-ion batteries, J. Mater. Chem. 21 (2011) 9891–9911.
[76] K. Szubert, J. Wojciechowski, L. Majchrzycki, W. Jurczak, G. Lota, H. Maciejewski, The rapeseed oil based organofunctional silane for stainless steel protective coatings, Materials (Basel) 13 (2020) 2212.
[77] A. Lasia, Electrochemical Impedance Spectroscopy and its Applications, Springer, New York, NY, 2015.
[78] E. Barsoukov, J.R. Macdonald, Impedance Spectroscopy: Theory, Experiment, and Applications, 2nd Edition, 2 ed., Wiley, 2005.
[79] X. Yuan, Z.F. Yue, X. Chen, S.F. Wen, L. Li, T. Feng, EIS study of effective capacitance and water uptake behaviors of silicone-epoxy hybrid coatings on mild steel, Prog. Org. Coat. 86 (2015) 41–48.
[80] B. Hirschorn, M.E. Orazem, B. Tribollet, V. Vivier, I. Frateur, M. Musiani, Determination of effective capacitance and film thickness from constant-phase-element parameters, Electrochim. Acta 55 (2010) 6218–6227.
[81] A. Kocijan, D.K. Merl, M. Jenko, The corrosion behaviour of austenitic and duplex stainless steels in artificial saliva with the addition of fluoride, Corros. Sci. 53 (2011) 776–783.
[82] H. Luo, H.Z. Su, C.F. Dong, K. Xiao, X.G. Li, Influence of pH on the passivation behaviour of 904L stainless steel bipolar plates for proton exchange membrane fuel cells, J. Alloy Compd. 686 (2016) 216–226.
[83] J. Bisquert, G. Garcia-Belmonte, P. Bueno, E. Longo, L.O.S. Bulhoes, Impedance of constant phase element (CPE)-blocked diffusion in film electrodes, J. Electroanal. Chem. 452 (1998) 229–234.
[84] J.P. Diard, C. Montella, Diffusion-trapping impedance under restricted linear diffusion conditions, J. Electroanal. Chem. 557 (2003) 19–36.
[85] E. Remita, A. Boughrara, B. Tribollet, V. Vivier, E. Sutter, F. Ropital, J. Kittel, Diffusion impedance in a thin-layer cell: experimental and theoretical study on a large-disk electrode, J. Phys. Chem. C 112 (2008) 4626–4634.